Published in final edited form as:
J Immunol. 2013 November 15; 191(10): . doi:10.4049/jimmunol.1301958.

MAIT recognition of a stimulatory bacterial antigen bound to MR11

Jacinto López-Sagaseta[*], **Charles L. Dulberger**[*], **Amanda McFedries**[†], **Mark Cushman**[‡], **Alan Saghatelian**[†], and **Erin J. Adams**[*,§]

[*]Department of Biochemistry and Molecular Biology, University of Chicago, Chicago, IL, 60637, USA

[†]Department of Chemistry and Chemical Biology, Harvard University, Cambridge, MA, 02138, USA

[‡]Department of Medicinal Chemistry and Molecular Pharmacology, College of Pharmacy, and The Purdue Center for Cancer Research, Purdue University, West Lafayette, IN 47907, United States

[§]Committee on Immunology, University of Chicago, Chicago, IL, 60637, USA

Abstract

MR1-restricted Mucosal Associated Invariant T (MAIT) cells represent a sub-population of αβ T cells with innate-like properties and limited TCR diversity. MAIT cells are of interest due to their reactivity against bacterial and yeast species, suggesting they play a role in defense against pathogenic microbes. Despite the advances in understanding MAIT cell biology, the molecular and structural basis behind their ability to detect MR1-antigen complexes is unclear. Here we present our structural and biochemical characterization of MAIT TCR engagement of MR1 presenting an *E. coli*-derived stimulatory ligand, rRL-6-CH_2OH previously found in *Salmonella typhimurium*. We show a clear enhancement of MAIT TCR binding to MR1 due to presentation of this ligand. Our structure of a MAIT TCR/MR1/rRL-6-CH_2OH complex shows an evolutionarily conserved binding orientation, with a clear role for both the CDR3α and CDR3β loops in recognition of the rRL-6-CH_2OH stimulatory ligand. We also present two additional xeno-reactive MAIT TCR/MR1 complexes that recapitulate the docking orientation documented previously despite having variation in the CDR2β and CDR3β loop sequences. Our data supports a model by which MAIT TCRs engage MR1 in a conserved fashion, their binding affinities modulated by the nature of the MR1 presented antigen or diversity introduced by alternate Vβ usage or CDR3β sequences.

Introduction

Mucosal Associated Invariant T (MAIT) cells are an evolutionarily conserved subpopulation of αβ T cells in mammals that are characterized by the expression of a semi-invariant αβ T cell receptor and restriction to the MHC-like protein MR1 (1-3). MAIT cells exhibit an innate-like phenotype and are found predominantly in mucosal tissues such the gut lamina propria and the lung. MAIT cells are also found at high frequency in the liver and in blood they can represent up to 10% of the CD4-αβ T cell population (4, 5). MAIT cell

[1]This study was supported by National Institutes of Health Grant R01AI073922 (to E.J.A.).

Correspondence should be addressed to: Erin J. Adams, 929 E. 57th Street, GCIS W236, Department of Biochemistry and Molecular Biology, University of Chicago, Chicago, IL, 60637., Telephone: 773-834-9816, Fax: 773-702-0439, ejadams@uchicago.edu.

development is dependent on MR1 expression, B cells and an established host commensal flora (2, 6).

Highly conserved across mammalian evolution, MR1 transcripts and protein are detected in most tissues, yet detection on the cell surface is low or undetectable under basal conditions (7, 8). The recent structural elucidation of MR1 (9, 10) revealed an overall backbone structure similar to peptide-presenting, classical MHC molecules, but with a putative antigen binding cavity of smaller dimensions due to the presence of large aromatic and basic residues lining the cavity. The aromatic architecture of this cavity is complementary to the small, ring-structure containing ligands identified recently (10) that are derivatives of two B-vitamin metabolic pathways, folic acid (vitamin B9) and riboflavin (vitamin B2). 6-Formylpterin (6-FP) was identified as an MR1-bound ligand, potentially covalently attached via Schiff base to lysine 43 found in the ligand-binding cavity of MR1. 6-FP was non-stimulatory to MAIT cells. In contrast, 6,7-dimethyl-8-ribityllumazine (DMRL), the direct precursor to riboflavin, and two DMRL variants were identified as MR1 ligands sufficient to stimulate MAIT cells.

To engage an MR1-antigen complex, human MAIT cells use an αβ TCR composed of a mostly invariant α chain (Vα7.2/Jα33) that associates with a limited array of βchains: Vβ2, Vβ13 and Vβ22, amongst others (11). Diversity in the variable domain of the β-chain arises from Vβ-Dβ-Jβ gene segment rearrangement which generates highly variable CDR3β loops, conferring MAIT TCRs a certain level of diversity despite the Vβ restriction. MAIT cells can be activated upon infection with diverse bacterial or yeast species including Eschericia coli, Staphylococcus aureus, Mycobacterium tuberculosis, Salmonella typhimurium, Candida albicans and *Saccharomyces cerevisiae* but not viruses (5, 12). Human MAIT cell autoreactivity has also been described in MR1-transfected cells in a microbial-independent manner (7, 13, 14), suggesting that endogenous ligands can contribute to MAIT cell reactivity.

Taking advantage of a ligand-independent, cross-species reactivity between human MAIT cells and bovine MR1, our group recently reported the first crystal structure of a complex between a MAIT TCR and MR1, providing a molecular model for how MAIT cells engage their MR1 ligand (9). This model was consistent with mutagenesis of the MAIT TCR/MR1 interaction from other groups (14, 15), and superimposes almost identically with a recently reported complex structure of a human MAIT TCR with human MR1 (16), supporting it as a *bon fide* model for MAIT TCR engagement of MR1. In this complex, the MAIT TCR bound in a diagonal fashion, reminiscent of classical αβ TCR recognition of MHC-peptide complexes (17) and Type II Natural Killer T (NKT) cell recognition of CD1d (18, 19). This docking orientation positioned the CDR3 loops of both the α and β chains close to the opening of the ligand-binding cavity. Modeling of the stimulatory ligands identified by Kjer-Nielsen and colleagues (10) into this complex suggested an important role for Tyr95 of the CDR3α loop, as this residue was positioned directly over the opening of this cavity, in hydrogen-bonding proximity to the ribityl chain of the stimulatory compounds DMRL and reduced 6-hydroxymethyl-8-(1-D-ribityl)lumazine (rRL-6-CH_2OH). This complex also identified the three residues on MR1 mediating the human/cow cross-reactivity.

Here, we present our results derived from an engineered, humanized version of bovine MR1 (hbMR1) that was expressed recombinantly in insect cells exposed to *E. coli* culture supernatant (*E. coli* sn) as a source of MAIT cell-reactive ligands. We demonstrate an enhancement of MAIT TCR binding to *E. coli*-loaded hbMR1 over unloaded and show through Mass Spectrometry (MS) that the bound MR1 ligand is rRL-6-CH_2OH. Furthermore, our complex of the F7 MAIT TCR with this rRL-6-CH_2OH-loaded MR1 provides critical information about how the MAIT TCR engages MR1 ligands, confirming a

pivotal role for Tyr95 of the CDR3α loop and establishing a role of the CDR3β loop in ligand binding. This complex, like our previously reported xeno-reactive complex, is strikingly similar to the recently reported human MAIT/MR1 complex with a highly similar stimulatory compound (16), reinforcing the evolutionary conservation of this interaction. Lastly, we present structural evidence that variation in Vβ usage and diversity in the sequence of the CDR3β loops does not affect TCR docking, but can modulate the affinity of binding to MR1 with and without stimulatory ligand through variable contacts with MR1 and ligand.

Materials and Methods

Recombinant protein expression and purification

hbMR1 was cloned, expressed and purified as previously described (9). Briefly, the triple mutant (hbMR1) was generated through overlapping PCR and cloned into the pAcGP67A vector (BD Biosciences) for subsequent expression via baculovirus in Hi5 cells. The recombinant protein was purified with Nickel NTA Agarose (Qiagen), anion exchange and size exclusion chromatography. For preparation of *E. coli* supernatant, BL21 cells were cultured overnight and then centrifuged at 6000 rpm for 30 minutes. The supernatant was then passed through a 10 kD cut-off membrane and the flow-through collected. Variable amounts from 10 to 100 ml of this flow-through were added every 24 hours to the Hi5s cells after infection with the recombinant baculovirus for hbMR1. The expression and purification of the MAIT TCR clones F7, G2 and AE6 was carried out in a similar way to previously described procedures for both Hi5 and *E. coli* expression systems (9, 20, 21).

Binding studies of MR1 and MAIT TCR interactions

For binding analysis between hbMR1 and the different human MAIT TCR clones, hbMR1 expressed in the presence or absence of the *E. coli* sn was captured to 4 μm units on a Ni-NTA™ (NTA) Biosensor in a Blitz System Package (Fortebio) as described before (9). The binding affinities for the F7, G2 and AE6 MAIT TCR clones were each tested by running increasing concentrations of the TCRs over the immobilized hbMR1 protein in 10 mM Hepes pH 7.4, 150 mM NaCl. IgG F_C was captured to a similar level and used to subtract non-specific binding signals. Subtracted responses were then used for calculating the affinity K_Ds with GraphPad Prism by plotting the binding values at equilibrium against the TCR concentrations.

Mass spectrometry analysis of hbMR1

Analysis of DMRL Standard (m/z 325.1154)—6.25 μg of DMRL (m/z 325.1154) was injected onto a Luna NH2 4.6×50 mm, 5 μm column. The flow was analyzed by ESI-TOF-MS on a Bruker maXis impact QTOF with Agilent 1290 HPLC using a binary gradient of 95% B to 0% over 5 minutes (A: 20 mM ammonium acetate in water, pH 9.0; B: acetonitrile). The target ion was detected after elution with aqueous gradient and data were collected in the negative ion mode. Retention time was obtained by extracted ion chromatogrphy of the respective m/z. Product ions were obtained by tandem MS with a collision energy of 20 eV. For hbMR1, comparison of hbMR1 protein that was exposed to *E. coli* sn and an untreated control hbMR1 sample were analyzed on a Bruker maXis impact QTOF LC/MS operating in the negative ion mode. 5 uL each of 25 μM hbMR1 was injected onto a Luna NH2 4.6×50 mm, 5 um column in 20 mM ammonium acetate, pH 9 buffer and eluted with an aqueous gradient as described above. The retention time of rRL-6-CH_2OH was determined by extracted ion chromatograms using the m/z values. Product ions were obtained from target fragmentation at collision-induced voltages of 20.

Ternary complex formation and crystallization

For crystallization purposes, F7, G2 and AE6 recombinant *E. coli*-derived heterodimeric MAIT TCRs were refolded and purified (9) and then stoichiometrically mixed with hbMR1 or bovine MR1 and concentrated to 5-10 mg/ml. Crystals of bovine MR1/F7 MAIT TCR complex were used for microseeding fresh sitting drops containing hbMR1/F7 MAIT TCR, bovine MR1/G2 MAIT TCR and bovine MR1/AE6 MAIT TCR and mother liquor consisting of 100 mM Hepes and variable concentrations of ammonium sulfate from 0.9 to 2.0 M. Crystals for all of the complexes appeared in times ranging from two to twelve weeks.

Crystallographic data collection, structure determination and refinement

Prior to data collection, crystals were soaked in mother liquor containing 20% glycerol and then cryo-cooled. All data sets were collected on a MAR300 CCD at beamline 23 ID-D and 23 ID-B at the Advanced Photon Source (APS) at Argonne National Laboratory and processed with HKL2000 (22). All datasets were corrected for anisotropic diffraction with the Phenix software suite (23). The structures of the ternary complexes were solved using the published complex structure of bovine MR1/F7 MAIT TCR (PDB 4IIQ) as a search model and removing the TCR CDR loops and all non-protein coordinates prior to molecular replacement with Phaser (24). The derived solution was refined with the Phenix.refine package (25) including Translation/Libration/Screw vibrational motions (26) at the latest stages of refinements, and combined with manual building in Coot (27) in between the refinement steps. When necessary, PRODRG (28) was used for the generation of ligand libraries and coordinates that were included in the refinement and building process. A random 5% of reflections were taken out for each data set for statistical validation purposes (Rfree) along the entire refinement processes.

Structure analysis

Intermolecular contacts and distances were calculated using the program Contacts from the CCP4 software package (29), interface surface areas were calculated using the PISA server (http://www.ebi.ac.uk/msd-srv/prot_int/pistart.html) and all structural figures were generated using the program Pymol (Schrödinger). Coordinates and structure factors have been deposited in the Protein Data Bank under the accession codes http://www.ncbi.nlm.nih.gov/pubmed/10592235:4LCC (F7 MAIT TCR/hbMR1),4L8S (G2 MAIT TCR/bMR1) and 4L9L (AE6 MAIT TCR/bMR1).

Results

MAIT TCRs show increased affinity for a humanized version of bovine MR1 (hbMR1) expressed in the presence of *E. coli* supernatant

Our initial attempts to recombinantly express human versions of MR1 in insect cells failed despite extensive attempts at engineering different constructs. Alternatively, we generated a humanized version of bovine MR1 (9), hbMR1, by mutating the three TCR contact positions that differ between human and bovine MR1 (Ala72Met in MR1 α1 helix and Arg147Gln and Gln151Leu in α2 helix), which we showed modulated MAIT cell xeno-reactivity (9). This construct expressed well and eluted as a monodispersed peak under size exclusion chromatography. We have used this construct in this study to characterize, structurally and biophysically, the recognition of a MAIT cell reactive ligand bound to hbMR1 by human MAIT TCRs.

Several studies have demonstrated MAIT cell reactivity against MR1-transfected APCs infected with different strains of bacteria and/or yeast (5, 10, 12, 14). One of the strains able to trigger MAIT cell response and activation is *Escherichia coli* (*E. coli*). We sought to

determine whether a stimulatory ligand could be loaded by expressing, in our insect expression system, our recombinant hbMR1 in the presence of *E. coli* supernatant (sn). Protein derived from this method had a noticeable yellow hue, consistent with the presence of a flavonoid substance. Using Bio-Layer Interferometry (BLI) we compared the binding kinetics of three MAIT TCRs to the *E. coli* loaded hbMR1 compared to that of hbMR1 expressed in the absence of *E. coli* sn (Figure 1). The binding studies demonstrated a twenty-fold increase in the binding affinity by the F7 MAIT TCR, more than 100-fold increase by the G2 MAIT TCR and a low micromolar affinity interaction for the AE6 MAIT TCR clone, whose interaction with the untreated hbMR1 was unmeasureable (Figure 1). These affinities (~4.5 uM and 4.9 uM) measured for the MAIT TCR interactions with hbMR1 loaded with a ligand derived from *E. Coli* supernatant are similar to those measured between MAIT TCRs with human MR1 loaded with synthetic rRL-6-CH_2OH (1.65 uM) (16). Differences between MR1 production strategies and ligand loading of these two studies might result in slight differences in affinity. These results suggest that hbMR1 is loaded with a ligand or ligands of bacterial origin that plays a direct role in enhancement of the recognition by the MAIT TCR.

The *E. coli* derived ligand bound by hbMR1 is rRL-6-CH_2OH

These results prompted us to analyze by mass spectrometry the content of the hbMR1 in both *E. coli* exposed and non-exposed protein samples. Normal phase QTOF analysis clearly identified a compound with a retention time of ~ 7 minutes present only in the *E. coli*-treated sample (Figure 2A). Mass spectrometry analysis of this compound determined a compound with a m/z ratio of 329.1095 and whose fragmentation yielded a pattern nearly identical to that found for rRL-6-CH_2OH (r-RL) (Figure 2B), a MAIT cell stimulatory ligand characterized from *Salmonella typhimurium* supernatant (10). This compound is generated as a by-product of the riboflavin synthesis pathway and its structure comprises a lumazine core and a ribityl chain (Figure 2A, inset). rRL-6-CH_2OH has been shown to trigger MAIT cell activation in an MR1-dependent manner, and displayed the strongest potency in activating MAIT cells among three structurally related compounds (10). Thus, the increased MAIT TCR affinity to the *E. coli*-treated hbMR1 sample correlates with the presence of this ribityl moiety, which our model suggested (9) directly participates in MAIT TCR recognition of MR1-presented antigen.

The crystal structure of the F7 MAIT TCR in complex with hbMR1 and rRL-6-CH_2OH demonstrates a conserved binding orientation

To determine the structural basis for this enhanced recognition of rRL-6-CH_2OH loaded hbMR1 by the MAIT TCR, we used our recombinantly expressed, rRL-6-CH_2OH loaded MR1 in crystallization screens with the F7 MAIT TCR. Single crystals grown with these components diffracted well and were used to collect a full data set that refined to 3.3 Å (Table 1). Overall, the docking mode of the MAIT TCR is highly similar to that observed with bovine MR1 (9) and human MR1 (16), with the MAIT TCR docking in a diagonal orientation with respect to the α1 and α2 helixes of hbMR1 (Figure 3A). The α chain CDR loops of the MAIT TCR mostly contact residues of the α2 helix of hbMR1, whereas the β chain is biased towards the α1 helix of hbMR1 (Figure 3B, 3C and Table 2). These contacts, with the exception of those made with the three bovine specific amino acids (A72, R147 and Q151), are remarkably similar between this complex and that of our previously reported MAIT/bMR1 complex (Supplementary Figure 1). Moreover, the TCR docking of both these complexes superimpose almost identically with the recently published human MAIT/MR1/RL-6-Me-7-OH complex (Figure 3B), further validating the evolutionary conservation of MAIT TCR recognition across species. The buried surface area (BSA) for the MAIT TCR-hbMR1 interface spans approximately 1070 $Å^2$ with 52% and 48% contributed by the α and β chains of the MAIT TCR, respectively (Figure 3C).

Previously, we reported a critical role for the CDR3α loop in the interaction with bMR1; this is confirmed in this complex, with Y95 of the CDR3α loop positioned directly over the ligand-binding cavity opening. The conformation of the CDR3α loop in this complex is essentially identical to the CDR3α loop conformations noted in the xeno-reactive complex (9) and the unliganded human MAIT TCR (15) as well as the human complex (16) (Supplementary Figure 2), confirming a critical role for Y95 in MAIT cell recognition of MR1/ligand and the rigidity of the CDR3α loop upon docking. In addition, we also see a role for the CDR3β loop in MR1 recognition due to a subtle shift in conformation, resulting in a new contact established with MR1 (G98β with Trp69 in the hbMR1 α1 helix). Discussed in more detail below, the CDR3β loop also makes a direct contact with the rRL-6-CH_2OH ligand, demonstrating a clear role for the diverse CDR3β loop in ligand discrimination. Despite the flexibility observed in the α2 helix in human MR1 (10), the structure with hbMR1 does not display evident differences in the backbone positioning, suggesting that hbMR1 does not require special conformational rearrangements to be engaged by a MAIT TCR (Supplementary Figure 3). Slight flexibility was noted in the α2 helix between the human MR1 unliganded (10) and liganded (16) structures however this may be in part due to the different resolutions of the datasets (3.2Å versus 2.0Å and 1.9Å).

Structural evidence for the involvement of the ribityl chain in rRL-6-CH_2OH recognition by a human MAIT TCR

Electron density for the rRL-6-CH_2OH ligand is unambiguous, in a position very similar to that of our model (9) (Figure 4A,) and that observed for 6-FP (9, 10), where the aromatic residues lining the cavity interact with the lumazine moiety primarily through van der Waals and pi-stacking interactions (Figure 4B). Hydrogen-bonds are noted between rRL-6-CH_2OH and several MR1 side chains: Ser24, Lys43, Arg94 and Tyr152 (Figure 4A and Table 2) and function to stably anchor the ligand in the ligand-binding cavity. The ribityl group extends upward towards the opening of the ligand-binding cavity, engaging the MAIT TCR through both the CDR3α and CDR3β loops. Y95 of the CDR3α loop establishes at least one hydrogen bond with the ribityl group, as we previously predicted (9). However in this complex we see a new role for the CDR3β loop in ligand discrimination. A hydrogen bond between the main chain nitrogen of the CDR3β Glu99 is established with the terminal hydroxyl of the ribityl chain of rRL-6-CH_2OH. These contacts provide a clear rational for the enhancement of MAIT cell binding upon recognition of MR1 loaded with stimulatory ligands such as rRL-6-CH_2OH. The conformation of the RL-6-Me-7-OH ligand (16) recently reported in human MR1 is flipped in relation to the conformation of rRL-6-CH_2OH reported here, resulting in the ribityl chain of RL-6-Me-7-OH being more sequestered in the MR1 binding cavity (Figure 4C). This is unlikely due to differences in the MR1 binding pockets as the position of the residues in the two structures superimpose almost perfectly (Figure 4C). The positioning of the RL-6-Me-7-OH ligand in human MR1 results in only TCR contact, Y95 of the CDR3α loop. This likely is the reason for the reduced functional potency of this ligand in relation to rRL-6-CH_2OH (10) and strongly suggests that ligands presented by MR1 adopt unique conformations in the ligand binding cavity that are dependent on their chemical structure; these conformations can have direct effects on the functional outcome.

Ligand-induced conformational change in CDR3β

To determine whether conformational adjustments play a role in MAIT TCR surveillance of MR1-presented antigens, we compared our crystal structure of the F7 MAIT TCR in complex with hbMR1/rRL-6-CH_2OH to that of F7 in complex with bovine MR1. A small conformational shift of the CDR3β loop was observed, resulting in a hydrogen bond between Gly98β and the Trp69 side chain of hbMR1 (Figure 3C and Figure 5). These contacts are remote from the three species-specific differences noted in bovine MR1,

therefore it is unlikely that the sequence differences are the cause of this conformational change. Instead, it is more likely that conformational flexibility of the CDR3β loop plays a role in engagement of certain MR1-presented stimulatory ligands. As noted previously, the CDR3β loop does not contact the RL-6-Me-7-OH ligand (16) despite having the same amino acid sequence. The overall Cα backbone structure of hbMR1 compared with that of bovine MR1 is 1.0 RMSD, suggesting that hbMR1 does not change substantially upon presentation of a stimulatory ligand, or upon engagement of a MAIT TCR (Supplementary Figure 3).

Variation in MAIT TCR β chain usage results in unique contacts with MR1

We have demonstrated previously that variation in the β chain, either through Vβ domain usage or diversity at the CDR3β loop, can modulate the affinity of the MAIT TCR for MR1 (9). The three MAIT TCRs we previously examined, F7, G2 and AE6 clones all differ in their CDR3β loop sequences, however, F7 and G2 both use Vβ13.3 (TRBV6-1) and therefore share the same CDR1β and CDR2β sequences whereas AE6 uses Vβ13.2 (TRBV6-2), which differs in both the CDR1β and CDR2β sequences. F7 and G2 have similar binding affinities to bovine MR1 (30-40μM), but AE6 binding is approximately two-fold weaker (~70 μM) (9). This is also reflected in the measured affinities to hbMR1/rRL-6-CH_2OH, where F7 and G2 bind with ~5 μM affinity and AE6 is approximately two-fold weaker (8.2 μM) (Figure 1). To understand the molecular basis for our measured affinity difference and the role of Vβ and CDR3β diversity in MR1 binding, we determined the crystal structures of the G2 and AE6 MAIT TCRs in complex with bovine MR1 to 2.9 Å and 3.4 Å, respectively (Table 1, Figure 6 and Supplementary Figure 4).

Comparison of the three xeno-reactive structures shows a conserved docking mode despite variation in the Vβ domain usage and CDR3β loop sequence (Figure 6). Contacts of the CDR loops from the α chains are essentially identical, with minor contact differences attributable to the range of resolutions of these complexes. However, variation in contacts of the β chain were much more extensive. In the F7 complex with bovine MR1 no contacts with the CDR1β loop were observed (9), whereas in both G2 and AE6 the CDR1β loop is involved in MR1 recognition (Figure 6). In the G2 complex, there is only one VDW contact: Asn30 of CDR1β contacts Gln71 of the MR1 α1 helix. The AE6 TCR, however, makes more extensive contacts through the CDR1β loop, with three VDW contacts through Glu30 (with Gly68, Gln71 and Ala72 of the MR1 α1 helix) and one through Tyr31 with Leu65 of the MR1 α1 helix. Glu30 and Tyr31 are amino acid residues unique to the Vβ13.2 domain, suggesting that Vβ encoded sequence variation can play a significant role in MR1 recognition.

Variable positions in the CDR2β loop between Vβ13.3 and Vβ13.2 are also involved in MR1 binding (Figure 6). In the F7 complex structure, the CDR2β loop has extensive contacts with the α1 helix of MR1 (9); a highly similar set of contacts is also seen in the G2 complex, which shares the same Vβ domain (Vβ13.3), resulting in main-chain loop conformations that are superimposable. AE6, in contrast, establishes fewer contacts through the CDR2β loop and two of the loop contact residues (Val50 and Ala56) differ from the sequence of F7 and G2 (Ala50 and Asp56). Overall, the AE6 TCR appears to distribute its Vβ contacts over all CDR loops, unlike the CDR2β and CDR3β loop bias observed in F7 and G2.

Finally, all three TCRs differ in the amino acid sequences of their CDR3β loops and adopt different constellations of contacts with MR1. All CDR3β loops bridge the ligand-binding cavity, with contacts observed between both the α1 and α2 helices of MR1 (Figure 6, lower panel). The CDR3β loop of the F7 TCR is biased towards the α2 helix of MR1, with six VDW contacts and two hydrogen-bonds. Only four VDW contacts are made with the α1 helix of MR1 (9). In contrast, the G2 TCR CDR3β loop establishes the majority of contacts (five of six) with the α1 helix; four of these are VDW contacts and one, $Asp97^{O}$ with

Trp69$^{N\varepsilon 1}$, is a hydrogen-bond (Table 3). Of note is a salt-bridge established between Asp97 of the CDR3β and Arg61 of the α1 helix. Pro98β is the only CDR3β residue that contacts the α2 helix, hydrogen-bonding with Glu149$^{N\varepsilon 1}$. In the AE6 MAIT TCR clone, the contacts are distributed between the α1 and α2 helices of MR1 and are composed of both hydrogen-bonds and VDW interactions (Table 4). Pro93 and Asp94 contact the α1 helix residues Leu65 and Trp69 whereas Gly95 and Gly96 contact His148, Glu149, and Tyr152 of the α2 helix.

Discussion

The evolutionary conservation of the MAIT lineage and the molecule to which they respond suggests that this surveillance provides an important function in host protection and/or homeostasis. Yet the modulation of MAIT cell reactivity by MR1-presented ligands has remained unclear. The recent identification of small, ring-based molecules as ligands for MR1 and antigens for MAIT cells (10) has expanded our understanding of the signals that are used to engage the MAIT population and opens up a new class of potential MR1 ligands for MAIT cell modulation. Here, we provide structural, biochemical and biophysical data revealing the molecular basis of MAIT cell recognition of an MR1-presented stimulatory ligand and how diversity in the MAIT cell population via alternative Vβ gene usage and CDR3β loop diversity can further modulate MAIT cell recognition of MR1/ligand. This work provides a foundation upon which to study presentation of other MR1-presented antigens and determine how variation in the MAIT population translates into antigen recognition and effector function.

Our crystal structure of the F7 MAIT TCR in complex with hbMR1 loaded with *E. coli*-derived rRL-6-CH_2OH demonstrates a highly conserved docking orientation that is similar to the unconventional non-invariant NKT TCR-CD1d-sulfatide (18, 19) or classical αβ TCR-MHC-peptide complexes (17), both of which utilize diversity in their CDR3 loops to probe their variable antigens. The docking of the TCR onto MR1 is nearly identical to that observed in our ligand-independent, xeno-reactive complex (9), and the recently described human MAIT/MR1 complex (16) with a related but different stimulatory ligand, reinforcing the evolutionary conservation of this interaction and strongly suggesting that the TCR docking footprint does not vary with MR1-presented ligands.

Our structural data also reveal the orientation of the stimulatory rRL-6-CH_2OH in the hbMR1 binding cavity. Very similar to our predicted model and to the placement of the folic acid derivative 6-FP (9, 10), rRL-6-CH_2OH is surrounded by a cluster of aromatic MR1 residues and hydrogen-bonds with Ser24, Lys43 and Arg94 side chains in the hbMR1 groove. The ribityl chain emerges from the MR1 cavity, establishing hydrogen-bonds with both the CDR3α and β loops of the MAIT TCR. These additional contacts contributed by antigen to the interaction are consistent with the enhanced binding of MAIT TCRs with rRL-6-CH_2OH-loaded MR1. This orientation is different from that of the RL-6-Me-7-OH ligand resolved recently (16), and provides and excellent explanation for why this ligand is more stimulatory than RL-6-Me-7-OH. Additional ligand contacts with the CDR3β loop likely enhance TCR engagement resulting in the observed enhanced potency. The diversity in ligand conformations also suggests that the MR1 binding cavity can accommodate a range of structures, suggesting that other small molecules may serve as stimulatory ligands presented by MR1 to MAIT cells.

In our hbMR1-rRL-6-CH_2OH/MAIT TCR complex, the MAIT TCR straddles both MR1 α helices, positioning the semi-invariant CDR3α loop and highly diverse CDR3β loop over the opening of the MR1 ligand-binding cavity. Observed contacts between both CDR3 loops and the rRL-6-CH_2OH ligand confirm their importance in antigen recognition and suggest

that MAIT TCRs use both conserved amino acid motifs (Y95 in the CDR3α loop) and diversity (CDR3β loop residues) to probe MR1-presented antigens. The enhancement of MAIT TCR binding affinity when MR1 presents rRL-6-CH_2OH (20-to 100-fold enhancement over unloaded MR1) confirms the importance of these ligand contacts in MAIT TCR recognition of MR1. It is unknown whether the differences in the measured affinities between MAIT TCRs will dictate the effector function of the cell, or whether TCR diversity directs specificity to particular MR1-presented ligands. However, our demonstration that MAIT TCRs can recognize MR1-presented antigens with different affinities suggests that MAIT TCR diversity, either through use of alternate Vβ domains or variation within the CDR3β loop, plays an important role in MAIT cell surveillance. Perhaps TCR variability allows MAIT cells to tune their response to different MR1-presented antigens, or may imply alternate functions for MAIT cells in host defense or homeostasis that require a different affinity threshold for activation.

The complexes between the G2 and AE6 TCRs and bovine MR1 provide additional new insight into the role of β chain variation in MR1 recognition. Combined with the F7/bMR1 complex, we have three unique MAIT TCR/MR1 structures for comparison. These structures reveal that variation in the Vβ domain can modify contacts mediated through the CDR1β and CDR2β loops, as seen in the AE6 TCR, which uses Vβ13.2 instead of Vβ13.3. AE6 distributes its Vβ contacts over its CDR1 and CDR2 β loops, whereas F7 and G2 contacts are either exclusive to (F7), or heavily biased towards (G2) the CDR2β loop. Loop-swapping experiments have shown the importance of the CDR3β loop (15) but our structures reveal how each TCR establishes a novel constellation of contacts with MR1. Our finding that flexibility in the CDR3β loop plays an important role in MR1/ligand engagement contrasts with the essentially rigid docking of the α chain CDR loops onto the MR1/ligand surface.

Future directions that extend from this work include determining the identity of the MAIT cell-selecting ligand(s) presented by MR1 during MAIT cell development in the thymus. How is ligand involved in this recognition, or does it serve to merely stabilize MR1 expression on the cell surface? Are there endogenous ligands presented by MR1 that are associated with the reported MAIT cell involvement in autoimmune disorders (30-32)? And finally, given the reported evidence for the infiltration of Vα7.2-Jα33 MAIT cells in kidney and brain tumors (33), are there tumor-derived antigens mediating MAIT cell activity in these diseases? Our structures provide a molecular model by which ligand presentation by MR1 can be studied in each of these areas and, importantly, shed light into the role of MAIT TCR diversity in engagement of MR1-presented antigens.

Supplementary Material

Refer to Web version on PubMed Central for supplementary material.

Acknowledgments

We thank the staff of the Advanced Proton Source at GM/CA-CAT (23ID) for their use and assistance with X-ray beamlines; Ruslan Sanishvili, Steven Corcoran, and Michael Becker in particular for help and advice during data collection. We also sincerely thank Prof. Adelbert Bacher, Institute of Biochemistry and Food Chemistry, Food Chemistry Division, University of Hamburg, Germany for very helpful discussions and assistance with experimental plans.

References

1. Tilloy F, Treiner E, Park SH, Garcia C, Lemonnier F, de la Salle H, Bendelac A, Bonneville M, Lantz O. An invariant T cell receptor alpha chain defines a novel TAP-independent major

histocompatibility complex class Ib-restricted alpha/beta T cell subpopulation in mammals. J Exp Med. 1999; 189:1907–1921. [PubMed: 10377186]

2. Treiner E, Duban L, Bahram S, Radosavljevic M, Wanner V, Tilloy F, Affaticati P, Gilfillan S, Lantz O. Selection of evolutionarily conserved mucosal-associated invariant T cells by MR1. Nature. 2003; 422:164–169. [PubMed: 12634786]
3. Porcelli S, Yockey CE, Brenner MB, Balk SP. Analysis of T cell antigen receptor (TCR) expression by human peripheral blood CD4-8-alpha/beta T cells demonstrates preferential use of several V beta genes and an invariant TCR alpha chain. J Exp Med. 1993; 178:1–16. [PubMed: 8391057]
4. Dusseaux M, Martin E, Serriari N, Peguillet I, Premel V, Louis D, Milder M, Le Bourhis L, Soudais C, Treiner E, Lantz O. Human MAIT cells are xenobiotic-resistant, tissue-targeted, CD161hi IL-17-secreting T cells. Blood. 2011; 117:1250–1259. [PubMed: 21084709]
5. Gold MC, Cerri S, Smyk-Pearson S, Cansler ME, Vogt TM, Delepine J, Winata E, Swarbrick GM, Chua WJ, Yu YY, Lantz O, Cook MS, Null MD, Jacoby DB, Harriff MJ, Lewinsohn DA, Hansen TH, Lewinsohn DM. Human mucosal associated invariant T cells detect bacterially infected cells. PLoS Biol. 2010; 8:e1000407. [PubMed: 20613858]
6. Martin E, Treiner E, Duban L, Guerri L, Laude H, Toly C, Premel V, Devys A, Moura IC, Tilloy F, Cherif S, Vera G, Latour S, Soudais C, Lantz O. Stepwise development of MAIT cells in mouse and human. PLoS Biol. 2009; 7:e54. [PubMed: 19278296]
7. Huang S, Martin E, Kim S, Yu L, Soudais C, Fremont DH, Lantz O, Hansen TH. MR1 antigen presentation to mucosal-associated invariant T cells was highly conserved in evolution. Proc Natl Acad Sci U S A. 2009; 106:8290–8295. [PubMed: 19416870]
8. Riegert P, Wanner V, Bahram S. Genomics, isoforms, expression, and phylogeny of the MHC class I-related MR1 gene. J Immunol. 1998; 161:4066–4077. [PubMed: 9780177]
9. Lopez-Sagaseta J, Dulberger CL, Crooks JE, Parks CD, Luoma AM, McFedries A, Van Rhijn I, Saghatelian A, Adams EJ. The molecular basis for Mucosal-Associated Invariant T cell recognition of MR1 proteins. Proc Natl Acad Sci U S A. 2013; 110:E1771–1778. [PubMed: 23613577]
10. Kjer-Nielsen L, Patel O, Corbett AJ, Le Nours J, Meehan B, Liu L, Bhati M, Chen Z, Kostenko L, Reantragoon R, Williamson NA, Purcell AW, Dudek NL, McConville MJ, O'Hair RA, Khairallah GN, Godfrey DI, Fairlie DP, Rossjohn J, McCluskey J. MR1 presents microbial vitamin B metabolites to MAIT cells. Nature. 2012; 491:717–723. [PubMed: 23051753]
11. Le Bourhis L, Mburu YK, Lantz O. MAIT cells, surveyors of a new class of antigen: development and functions. Curr Opin Immunol. 2013; 25:174–180. [PubMed: 23422835]
12. Le Bourhis L, Martin E, Peguillet I, Guihot A, Froux N, Core M, Levy E, Dusseaux M, Meyssonnier V, Premel V, Ngo C, Riteau B, Duban L, Robert D, Huang S, Rottman M, Soudais C, Lantz O. Antimicrobial activity of mucosal-associated invariant T cells. Nat Immunol. 2010; 11:701–708. [PubMed: 20581831]
13. Huang S, Gilfillan S, Kim S, Thompson B, Wang X, Sant AJ, Fremont DH, Lantz O, Hansen TH. MR1 uses an endocytic pathway to activate mucosal-associated invariant T cells. J Exp Med. 2008; 205:1201–1211. [PubMed: 18443227]
14. Young MH, U'Ren L, Huang S, Mallevaey T, Scott-Browne J, Crawford F, Lantz O, Hansen TH, Kappler J, Marrack P, Gapin L. MAIT cell recognition of MR1 on bacterially infected and uninfected cells. PLoS One. 2013; 8:e53789. [PubMed: 23342002]
15. Reantragoon R, Kjer-Nielsen L, Patel O, Chen Z, Illing PT, Bhati M, Kostenko L, Bharadwaj M, Meehan B, Hansen TH, Godfrey DI, Rossjohn J, McCluskey J. Structural insight into MR1-mediated recognition of the mucosal associated invariant T cell receptor. J Exp Med. 2012; 209:761–774. [PubMed: 22412157]
16. Patel O, Kjer-Nielsen L, Le Nours J, Eckle SB, Birkinshaw R, Beddoe T, Corbett AJ, Liu L, Miles JJ, Meehan B, Reantragoon R, Sandoval-Romero ML, Sullivan LC, Brooks AG, Chen Z, Fairlie DP, McCluskey J, Rossjohn J. Recognition of vitamin B metabolites by mucosal-associated invariant T cells. Nature communications. 2013; 4:2142.
17. Garcia KC, Adams EJ. How the T cell receptor sees antigen--a structural view. Cell. 2005; 122:333–336. [PubMed: 16096054]

18. Girardi E, Maricic I, Wang J, Mac TT, Iyer P, Kumar V, Zajonc DM. Type II natural killer T cells use features of both innate-like and conventional T cells to recognize sulfatide self antigens. Nat Immunol. 2012; 13:851–856. [PubMed: 22820602]
19. Patel O, Pellicci DG, Gras S, Sandoval-Romero ML, Uldrich AP, Mallevaey T, Clarke AJ, Le Nours J, Theodossis A, Cardell SL, Gapin L, Godfrey DI, Rossjohn J. Recognition of CD1d-sulfatide mediated by a type II natural killer T cell antigen receptor. Nat Immunol. 2012; 13:857–863. [PubMed: 22820603]
20. Lopez-Sagaseta J, Kung JE, Savage PB, Gumperz J, Adams EJ. The Molecular Basis for Recognition of CD1d/alpha-Galactosylceramide by a Human Non-Valpha24 T Cell Receptor. PLoS Biol. 2012; 10:e1001412. [PubMed: 23109910]
21. Lopez-Sagaseta J, Sibener LV, Kung JE, Gumperz J, Adams EJ. Lysophospholipid presentation by CD1d and recognition by a human Natural Killer T-cell receptor. EMBO J. 2012; 31:2047–2059. [PubMed: 22395072]
22. Otwinowski Z, Minor W. Processing of X-ray diffraction data collected in oscillation mode. Methods Enzymol. 1997; 276:307–326.
23. Adams PD, Afonine PV, Bunkoczi G, Chen VB, Davis IW, Echols N, Headd JJ, Hung LW, Kapral GJ, Grosse-Kunstleve RW, McCoy AJ, Moriarty NW, Oeffner R, Read RJ, Richardson DC, Richardson JS, Terwilliger TC, Zwart PH. PHENIX: a comprehensive Python-based system for macromolecular structure solution. Acta Crystallogr D Biol Crystallogr. 2010; 66:213–221. [PubMed: 20124702]
24. McCoy AJ, Grosse-Kunstleve RW, Adams PD, Winn MD, Storoni LC, Read RJ. Phaser crystallographic software. J Appl Crystallogr. 2007; 40:658–674. [PubMed: 19461840]
25. Adams PD, A. PV, Bunkóczi G, Chen VB, Davis IW, Echools N, Headd JJ, Hung L-W, Kapral GJ, Grosse-Kunstleve RW, McCoy AJ, Moriarty NW, Oeffner R, Read RJ, Richardson DC, Richardson JS, Terwilliger TC, Zwart PH. PHENIX: a comprehensive Python-based system for macromolecular structure solution. Acta Cryst. D. 2010; 66:213–221. [PubMed: 20124702]
26. Painter J, Merritt EA. Optimal description of a protein structure in terms of multiple groups undergoing TLS motion. Acta Crystallogr D Biol Crystallogr. 2006; 62:439–450. [PubMed: 16552146]
27. Emsley P, Cowtan K. Coot: model-building tools for molecular graphics. Acta Crystallogr D Biol Crystallogr. 2004; 60:2126–2132. [PubMed: 15572765]
28. Schuttelkopf AW, van Aalten DM. PRODRG: a tool for high-throughput crystallography of protein-ligand complexes. Acta Crystallogr D Biol Crystallogr. 2004; 60:1355–1363. [PubMed: 15272157]
29. Collaborative Computational Project, N. The CCP4 Suite: Programs for Protein Crystallography. Acta Cryst. 1994; D50:760–763.
30. Miyazaki Y, Miyake S, Chiba A, Lantz O, Yamamura T. Mucosal-associated invariant T cells regulate Th1 response in multiple sclerosis. Int Immunol. 2011; 23:529–535. [PubMed: 21712423]
31. Croxford JL, Miyake S, Huang YY, Shimamura M, Yamamura T. Invariant V(alpha)19i T cells regulate autoimmune inflammation. Nat Immunol. 2006; 7:987–994. [PubMed: 16878136]
32. Illes Z, Shimamura M, Newcombe J, Oka N, Yamamura T. Accumulation of Valpha7.2-Jalpha33 invariant T cells in human autoimmune inflammatory lesions in the nervous system. Int Immunol. 2004; 16:223–230. [PubMed: 14734607]
33. Peterfalvi A, Gomori E, Magyarlaki T, Pal J, Banati M, Javorhazy A, Szekeres-Bartho J, Szereday L, Illes Z. Invariant Valpha7.2-Jalpha33 TCR is expressed in human kidney and brain tumors indicating infiltration by mucosal-associated invariant T (MAIT) cells. Int Immunol. 2008; 20:1517–1525. [PubMed: 18927318]

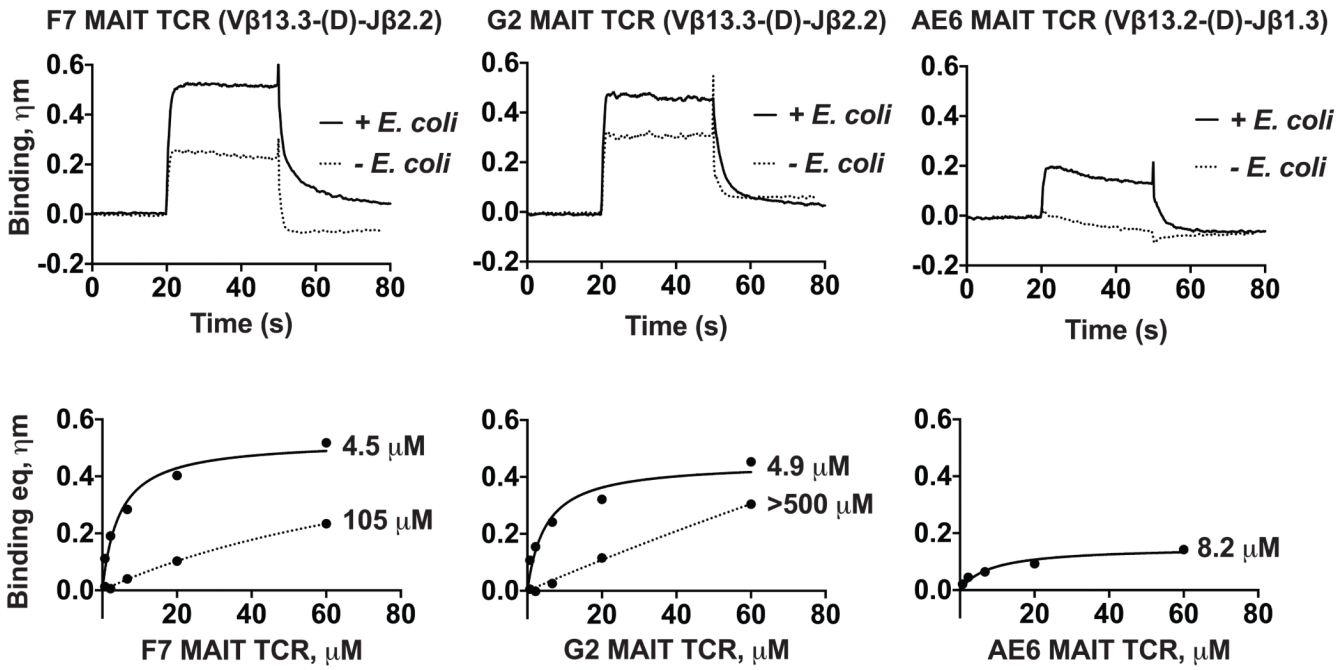

Figure 1.

Expression of hbMR1 in the presence of *E. coli* supernatant (sn) enhances the recognition by three different human MAIT TCRs. Upper panels, association and dissociation binding curves measured by Bio-Layer Interferometry (BLI) of three different human MAIT TCRs with hbMR1 expressed in the presence (+) or absence (-) of *E coli* sn. Shown for comparison are the binding curves for the highest concentrations of MAIT TCR tested, 60 μM. Bottom panels: non-linear regression fitting analysis of responses in equilibrium for each of the interactions.

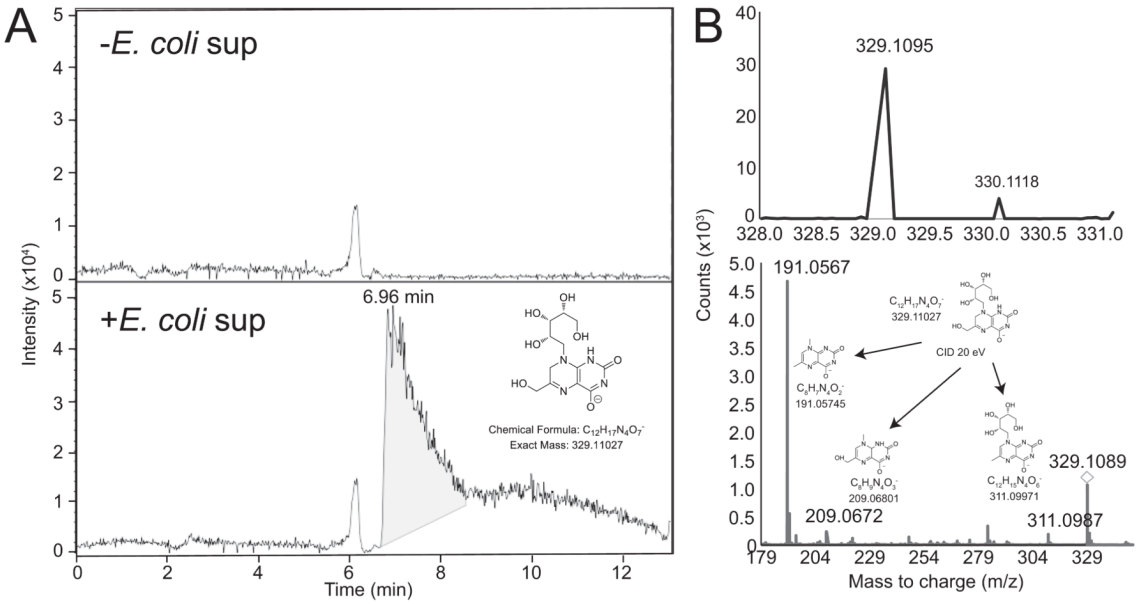

Figure 2.

Mass spectrometry reveals the presence of rRL-6-CH_2OH in the *E. coli*- treated hbMR1 sample. (A) Extracted ion chromatograms (EIC) for rRL-6-CH_2-OH (m/z 329.1103) from hbMR1 protein exposed to *E. coli* (bottom panel) compared to untreated protein control (upper panel). EIC shows compound with m/z 329.1103 present only in *E. coli* treated sample (inset). (B) Compound with m/z 329.1095 (top left) from the *E. coli*-treated hbMR1 sample and product ions from targeted fragmentation (bottom panel); displayed as insets are the structures of each of the products of the fragmentation. The precursor ion is indicated by a diamond. MS/MS product ion data matches against the theoretical fragmentation pattern of rRL-6-CH_2OH (top right) within < 5ppm.

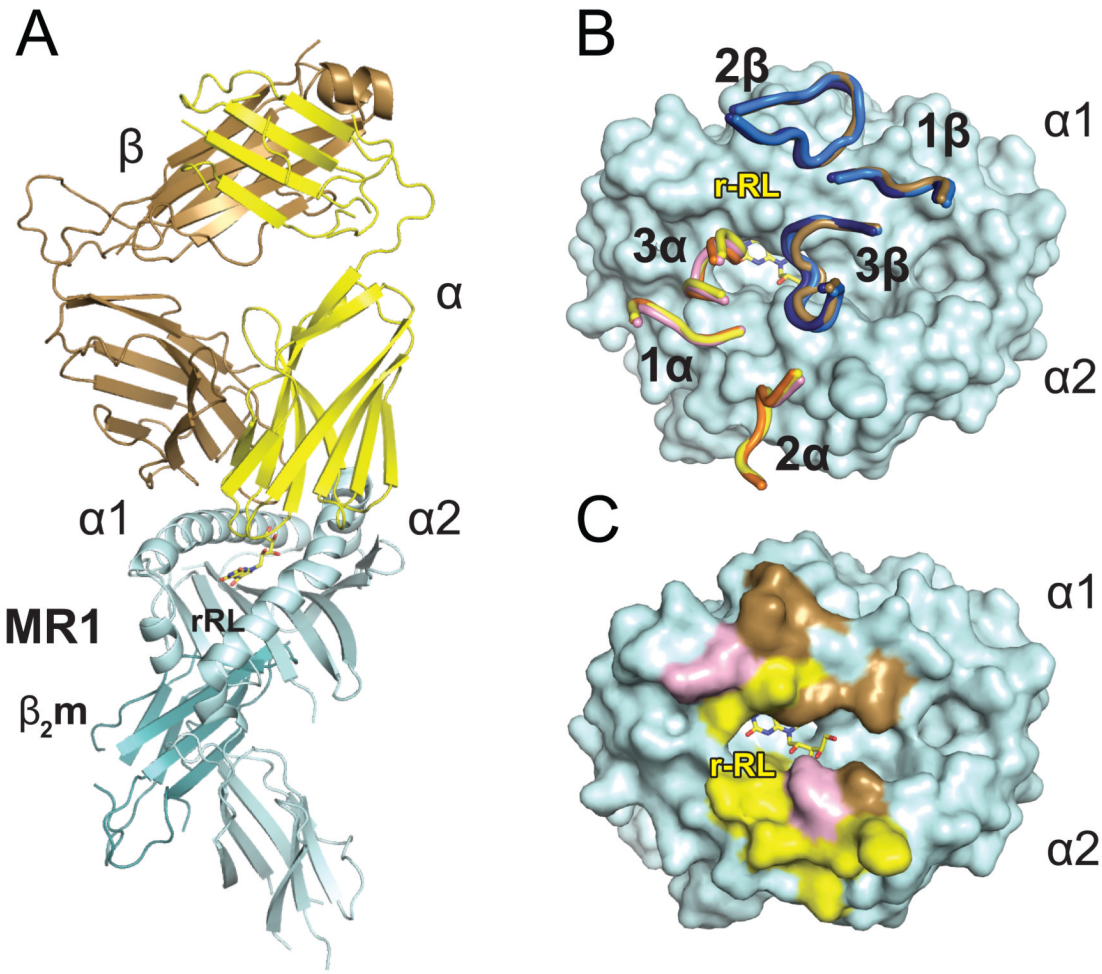

Figure 3.

MAIT TCR recognition of MR1-antigen. **A)** Cartoon diagram of the ternary complex structure human MAIT TCR/hbMR1 and the MAIT cell stimulatory ligand rRL-6-CH_2OH. The TCR α and β chains are shown respectively in yellow and brown colors, MR1 in cyan and β_2m in teal. rRL-6-CH_2OH is represented as yellow sticks. **B)** Superposition of the F7 MAIT TCR CDR loops in the complexes with bovine (shown in pink and marine for the α and β chains, respectively) and hbMR1 (shown in yellow and brown for the α and β chains, respectively) and comparison with the loop positioning in the human MAIT/MR1/RL-6-Me-7-OH complex (16) (loops shown in orange and dark blue for the α and β chains, respectively). All three complexes are aligned via MR1 and the respective CDR loops are displayed on top of the hbMR1 surface. **C)** Footprint of the F7 human MAIT TCR on hbMR1 surface. hbMR1 residues contacting the TCR α chain are shown in yellow and those contacting the β chain are shown in brown. Residues making contacts with both chains are in pink.

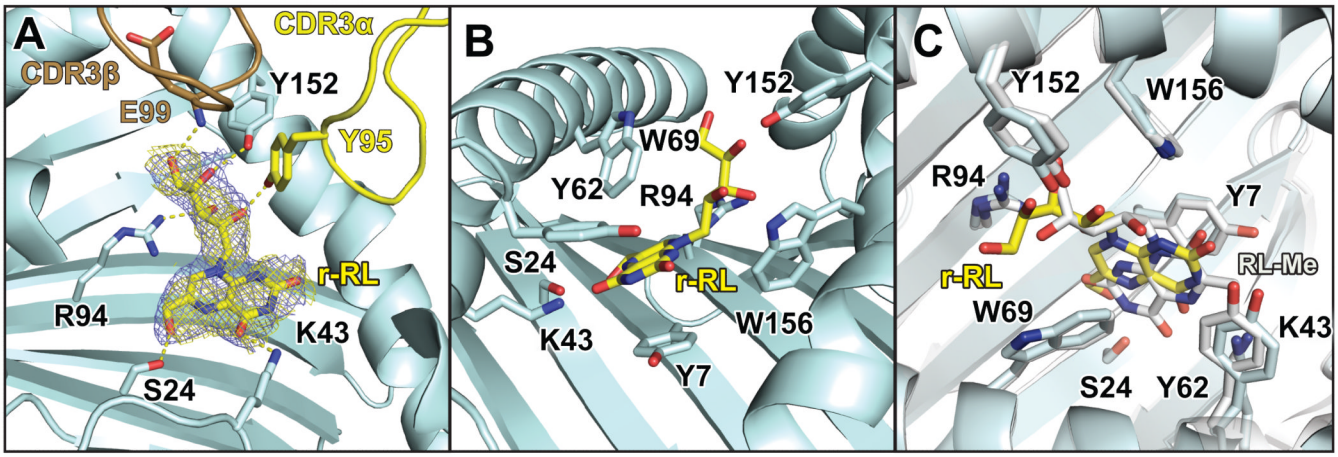

Figure 4.

Binding of rRL-6-CH_2OH in the MR1 pocket and contacts made within MR1 and with the MAIT TCR. A) electron density maps for rRL-6-CH_2OH bound in the MR1 groove. Simulated annealing omit map (yellow mesh) and $2F_0$-F_C electron density maps (violet) are displayed and contoured at 1σ together with the ligand, represented as sticks. Colors for hbMR1 and the TCR are as in previous figures. Hydrogen-bonds are highlighted in yellow dotted lines. B) view of rRL-6-CH_2OH and the hbMR1 polar and aromatic surrounding residues. C) Comparison of binding pocket residues between hbMR1 and human MR1 and positioning of the RL-6-Me-7-OH ligand (RL-Me) reported in (16) (shown in white).

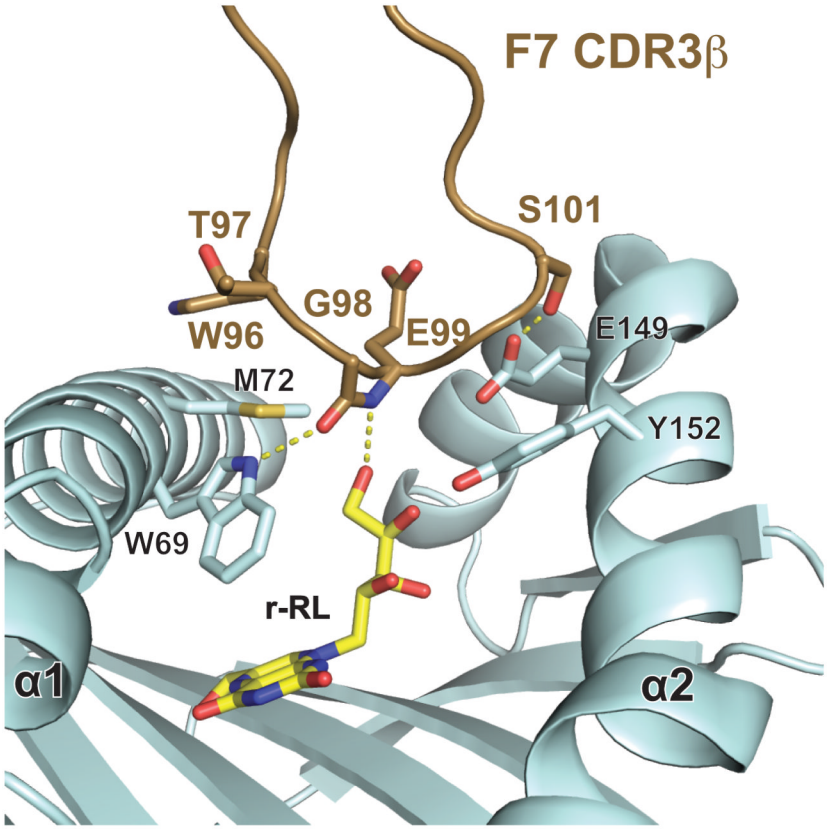

Figure 5.
The CDR3β loop demonstrates conformational flexibility in ligating hbMR1/rRL-6-CH_2OH. Shown in brown is the F7 MAIT TCR CDR3β loop bound to hbMR1/rRL-6-CH_2OH. Residues that make VDW and H-bond contacts are displayed as sticks, the later denoted by yellow dotted lines.

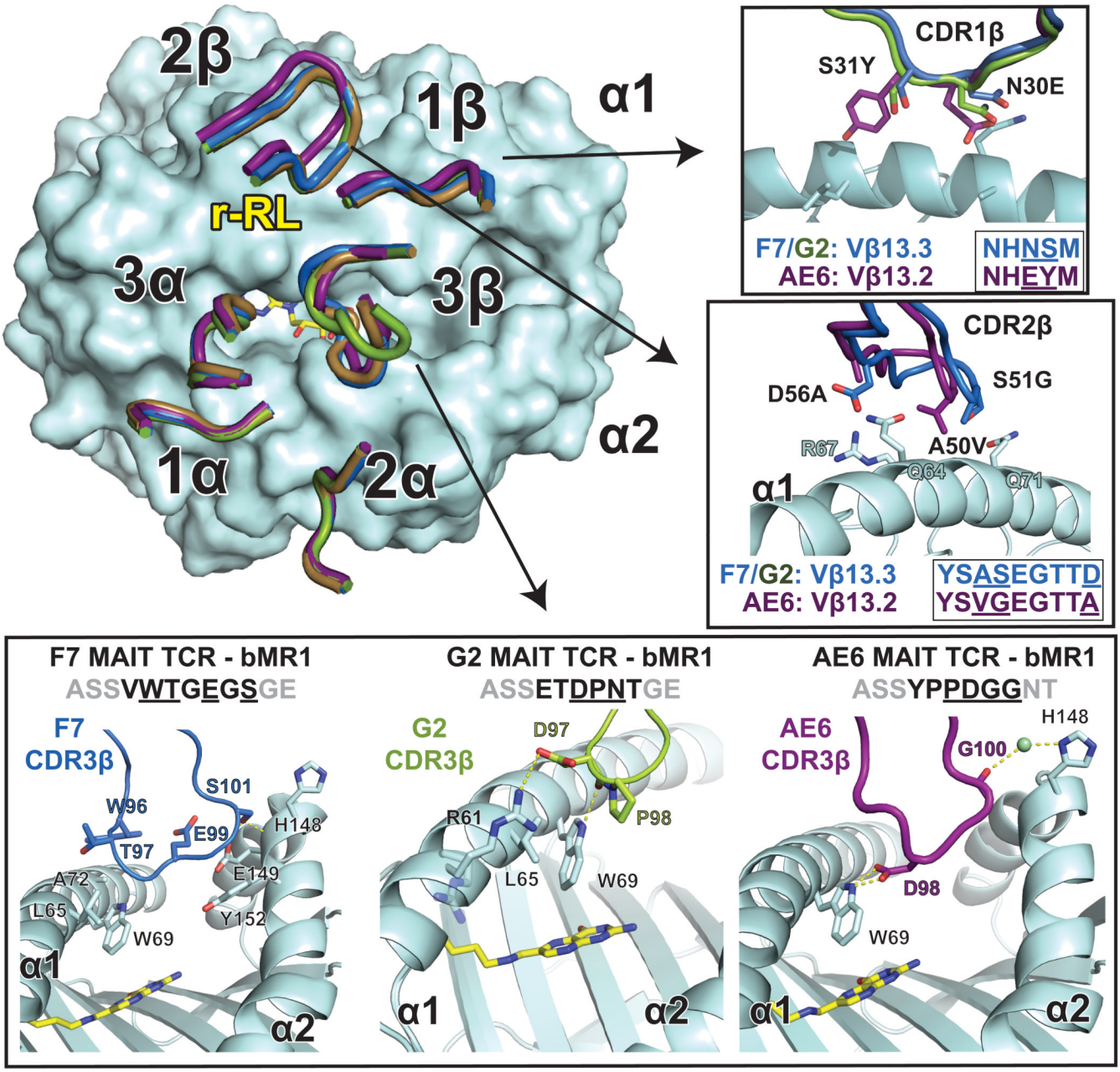

Figure 6.

Three different human TCRs adopt comparable docking modes despite different Vβ chain usage. Upper left: the CDR loops of the complexes between the G2 MAIT TCR (green) and AE6 MAIT TCR (purple) with bovine MR1 (cyan) are compared with the previously reported F7 MAIT TCR/bovine MR1 complex (TCR in brown, PDB ID: 4IIQ). The complexes were aligned via the main-chain Cα carbons of the MR1 heavy chain. Details of the residues differing between the TCRs are shown in insets: top: CDR1β, middle: CDR2β and bottom panel: CDR3β from each of the complexes. Sequences of the CDR loops are shown, with contact residues underlined. Hydrogen-bonds are indicated as yellow dashed lines.

Table 1
Data collection and refinement statistics (molecular replacement)

	MAIT TCR F7 hMR1-r-RL	MAIT TCR G2 Bovine MR1	MAIT TCR AE6 Bovine MR1
Data collection			
Space group	P 21 21 21	P 21 21 21	P 21 21 21
Cell dimensions			
a, b, c (Å)	85.9, 88.6, 155.5	83.1, 87.3, 155.8	82.8, 87.0, 156.3
α,β,γ (°)	90.00, 90.00, 90.00	90.00, 90.00, 90.00	90.00, 90.00, 90.00
Resolution (Å)	50 - 3.3 (3.36 - 3.3)	50 - 2.9 (2.95 - 2.9)	50 - 3.4 (3.46 - 3.4)
R_{merge}	0.072 (0.425)	0.068 (0.7)	0.128 (0.595)
I/σI	12.81 (3.92)	20.89 (2.88)	14.76 (5.35)
Completeness (%)	97.04 (78.29)	95.79 (93.02)	97.49 (80.54)
Redundancy	4.0 (4.1)	6.3 (6.0)	11.4 (9.9)
Refinement			
Resolution (Å)	3.3	2.9	3.4
Total No. Reflections	74945	155981	179796
No. Unique Reflections	18509	27400	15806
R_{work}/R_{free}	0.2548 / 0.3078	0.2433 / 0.2874	0.2560 / 0.3105
No. atoms			
Protein	5954	6288	6020
Ligand/ion	43	53	26
Water	1	8	1
B-factors			
Protein	83.70	74.50	91.90
Ligand	96.50	102.50	94.90
Waters	29.40	52.20	43.20
R.m.s. deviations			
Bond lengths (Å)	0.013	0.006	0.008
Bond angles (°)	1.26	0.70	0.99
Ramachandran favored (%)	96	96	96
Ramachandran outliers (%)	0.28	0	0.41

*Values in parentheses are for highest-resolution shell.

Table 2
Human F7 MAIT TCR contacts with hMR1-r-RL

α chain	MR1	Contact	β chain	MR1	Contact
CDR1			CDR2		
Gly28	Glu160	VDW	Tyr48	Arg61	VDW
Phe29	Glu160	VDW	Tyr48	Gln64	VDW
Phe29O	Asn155Nδ2	H-bond	Ala50	Gln64	VDW
Phe29N	Glu160Oε1	H-bond	Thr54	Gln64	VDW
Phe29O	Glu160Oε1	H-bond* (3.47)	Thr54	Arg67	VDW
Asn30	Tyr152	VDW	$Thr54^{O\gamma}$	$Gln64^{N\varepsilon 2}$	H-bond
Asn30	Asn155	VDW	$Thr54^{O\gamma}$	$Arg67^{N\eta 1}$	H-bond
Asn30	Trp156	VDW	Thr55	Gln64	VDW
Asn30	Glu160	VDW	Asp56	Gln64	VDW
$Asn30^{N\delta 2}$	$Asn155^{N\delta 2}$	H-bond* (3.55)	CDR3		
CDR2			Trp96	Met72	VDW
Tyr48	His148	VDW	Thr97	Trp69	VDW
Tyr48	Tyr152	VDW	Thr97O	$Trp69^{N\varepsilon 1}$	H-bond* (3.65)
Val50	Leu151	VDW	Gly98	Trp69	VDW
Val50	Tyr152	VDW	Gly98O	$Trp69^{N\varepsilon 1}$	H-bond
Val50	Asn155	VDW	Glu99	Glu149	VDW
Leu51	Leu151	VDW	Gly100	Tyr152	VDW
Leu51	Lys154	VDW	$Ser101^{O\gamma}$	$Glu149^{O\varepsilon 1}$	H-bond
Leu51	Asn155	VDW	Ser101N	Glu149Oε1	H-bond* (3.56)
$Glu55^{O\varepsilon 2}$	His148Nε2	H-bond	Ser101	Glu149	VDW
Glu55	His148	VDW			
Arg66	Asn155	VDW	**β chain**	**r-RL**	**Contact**
Arg66*Nη1*	Glu160Oε2	S-Bridge	Gly98	OAD,CAJ,	VDW
CDR3			Glu99	OAD	VDW
Ser93	Glu160	VDW	Glu99N	OAD	H-bond
$Ser93^{O\gamma}$	Glu160Oε2	H-bond			
Ser93	Trp164	VDW	**MP1**	**r-RL**	**Contact**
$Asn94^{N\delta 2}$	Arg61Nε	HB(	Tyr7	C4A,C4,O4,N3,N5	VDW
Asn94	Arg61	VDW	Phe8	OAC	VDW
Asn94	Tyr62	VDW	Arg9	CAI,C7,CAJ	VDW
$Asn94^{O\delta 1}$	$Tyr62^{OH}$	H-bond	Ser24	OAC,CAI	VDW
Tyr95	Leu65	VDW	$Ser24^{O\gamma}$	OAC	H-bond
Tyr95	Tyr152	VDW	Lys43	O4,C4	VDW
Tyr95	Trp156	VDW	Lys43 Nζ	N3	H-bond* (3.50)
$Tyr95^{OH}$	Tyr152OH	H-bond	Lys43 Nζ	O4	H-bond
$Tyr95^{OH}$	Trp156Nε1	H-bond* (3.73)	Tyr62	O2,N3	VDW
			Trp69	CAJ,C8A,C4A,N5	VDW
α chain	**r-RL**	**Contact**	Arg94	CAV,C7,CAT	VDW

α chain	MR1	Contact	β chain	MR1	Contact
Tyr95	OAF,OAE,CAU	VDW	Arg94	OAG	H-bond* (3.35)
Tyr95OH	OAF	H-bond	Ile96	OAG	VDW
Tyr95OH	OAE	H-bond* (3.60)	Tyr152	OAE,OAF	VDW
			Tyr152	OAE	H-bond
			Gln153	OAG	VDW
			Trp156	OAF,N1,CAK	VDW

Table 3
Human G2 MAIT TCR contacts with bovine MR1

α chain	MR1	Contact	β chain	MR1	Contact
CDR1			CDR1		
Gly28	Glu160	VDW	Asn30	Gln71	VDW
Phe29	Glu160	VDW	CDR2		
$Phe29^{O}$	$Asn155^{N\delta2}$	H-bond	Tyr48	Arg61	VDW
$Phe29^{N}$	$Glu160^{O\varepsilon1}$	H-bond* (3.42)	Tyr48	Gln64	VDW
$Phe29^{O}$	$Glu160^{O\varepsilon1}$	H-bond* (3.60)	Ala50	Gln64	VDW
Asn30	Tyr152	VDW	Ala50	Gly68	VDW
Asn30	Trp156	VDW	Ser51	Arg67	VDW
CDR2			Ser51	Gly68	VDW
Tyr48	His148	VDW	Glu52	Gln71	VDW
Tyr48	Tyr152	VDW	Thr54	Gln64	VDW
Val50	Leu151	VDW	Thr54	Arg67	VDW
Val50	Tyr152	VDW	$Thr54^{O\gamma}$	$Gln64^{N\varepsilon2}$	H-bond
Leu51	Leu151	VDW	$Thr54^{O\gamma}$	$Gln64^{O\varepsilon1}$	H-bond
Leu51	Lys154	VDW	$Thr54^{O\gamma}$	$Arg67^{N\varepsilon1}$	H-bond
Leu51	Asn155	VDW	Thr55	Gln64	VDW
$Glu55^{O\varepsilon2}$	Gln151	VDW	Thr55O	$Gln64^{N\varepsilon2}$	H-bond
Arg66	Asn155	VDW	Asp56	Gln64	VDW
$Arg66^{N\varepsilon}$	$Asn155^{O\delta1}$	H-bond* (3.51)	CDR3		
$Arg66^{N\eta1}$	$Glu159^{O\varepsilon2}$	S-Bridge	Asp97	Arg61	VDW
Arg66	Glu159	VDW	Asp97	Leu65	VDW
CDR3			Asp97	Trp69	VDW
Ser93	Glu160	VDW	Asp97O	$Trp69^{N\varepsilon1}$	H-bond
Asn94	Tyr62	VDW	Pro98	Trp69	VDW
$Asn94^{N\delta2}$	$Tyr62^{OH}$	H-bond	$Asn99^{N\delta2}$	$Glu149^{N\varepsilon1}$	H-bond
$Tyr95^{N}$	$Arg61^{N\eta1}$	H-bond* (3.62)			
Tyr95	Arg61	VDW			
Tyr95	Leu65	VDW			
Tyr95	Trp69	VDW			
Tyr95	Tyr152	VDW			
Tyr95	Trp156	VDW			
$Tyr95^{OH}$	$Tyr152^{OH}$	H-bond* (3.44)			
$Tyr95^{OH}$	$Trp156^{N\varepsilon1}$	H-bond			
Gln96	Arg61	VDW			
Gln96	$Arg61^{N\varepsilon}$	H-bond* (3.34)			

Table 4
Human AE6 MAIT TCR contacts with bovine MR1

α chain	MR1	Contact	β chain	MR1	Contact
CDR1			CDR1		
Gly28	Glu160	VDW	Glu30	Gly68	VDW
Phe29	Glu160	VDW	Glu30	Gln71	VDW
$Phe29^{O}$	$Asn155^{N\delta2}$	H-bond	Glu30	Ala72	VDW
$Phe29^{N}$	$Glu160^{O\varepsilon1}$	H-bond	Tyr31	Leu65	VDW
$Phe29^{O}$	$Glu160^{O\varepsilon1}$	H-bond* (3.53)	CDR2		
Asn30	Tyr152	VDW	Tyr48	Arg61	VDW
Asn30	Trp156	VDW	Tyr48	Gln64	VDW
Asn30	Trp160	VDW	Val50	Gln64	VDW
CDR2			Val50	Gly68	VDW
Tyr48	His148	VDW	Thr54	Arg67	VDW
Tyr48	Tyr152	VDW	$Thr54^{OH}$	$Arg67^{N\eta1}$	H-bond
Val50	Leu151	VDW	Thr54	Gln64	VDW
Val50	Tyr152	VDW	Thr55	Gln64	VDW
Leu51	Leu151	VDW	Lys67	Gln71	VDW
Leu51	Asn155	VDW	CDR3		
Glu55	His148	VDW	Pro93	Leu65	VDW
Glu55	His148	H-bond* (3.48)	Asp94	Trp69	VDW
Glu55	Gln151	VDW	$Asp94^{O\delta1}$	$Trp69^{N\varepsilon1}$	H-bond
Gly96	Tyr152	VDW	$Asp94^{O\delta2}$	$Trp69^{N\varepsilon1}$	H-bond
Arg66	Asn155	VDW	Gly95	Glu149	VDW
$Arg66^{N\varepsilon}$	$Asn155^{O\delta1}$	H-bond* (3.6)	Gly95	Tyr152	VDW
$Arg66^{N\eta1}$	$Glu159^{O\varepsilon2}$	S-Bridge	Gly96N	His148O	H-bond* (3.60)
Arg66	Glu159	VDW	Gly96O	$His148^{N\delta1}$	Water
CDR3			Gly96	Tyr152	VDW
Ser93	Glu160	VDW			
Ser93	Trp164	VDW			
$Ser93^{OH}$	$Glu160^{O\varepsilon2}$	H-bond			
Asn94	Tyr62	VDW			
Asn94	Trp164	VDW			
$Asn94^{N\delta2}$	Tyr62OH	H-bond			
$Tyr95^{N}$	$Arg61^{N\eta1}$	H-bond* (3.38)			
Tyr95	Arg61	VDW			
Tyr95	Leu65	VDW			
Tyr95	Trp69	VDW			
Tyr95	Tyr152	VDW			
Tyr95	Trp156	VDW			
$Tyr95^{OH}$	$Tyr152^{OH}$	H-bond			
$Tyr95^{OH}$	$Trp156^{N\varepsilon1}$	H-bond* (3.64)			

α chain	MR1	Contact	β chain	MR1	Contact
Gln96	Arg61	VDW			
$Gln96^{N\varepsilon 2}$	$Arg61^{N\varepsilon}$	H-bond* (3.59)			
$Gln96^{N}$	$Arg61^{N\eta 1}$	H-bond* (3.57)			